Ocean Systems Engineering, *Vol. 13, No. 4 (2023) 325-347*
https://doi.org/10.12989/ose.2023.13.4.325

Optimization of a numerical wave flume for efficient simulations

V. Kumaran*[1], A.V. Mahalingaiah[1], Manu[2] and Subba Rao[2]

[1]*Central Water &Power Research Station, (CWPRS), Pune 411 024, India*
[2]*Department of Water Resources and Ocean Engineering, National Institute of Technology, Karnataka, Surathkal, Mangalore-India- 575025*

(Received May 21, 2023, Revised August 15, 2023, Accepted August 22, 2023)

Abstract. The present work investigates the wave generation and propagation in a 2-D wave flume to assess the effect of wave reflection for varying beach slopes by using a numerical tool based on computational fluid dynamics. At first, a numerical wave flume (NWF) is created with different mesh sizes to select the optimum mesh size for time efficient simulation. In addition, different beach slope conditions are introduced such as 1:3, 1:5 and numerical beach at the far end of the NWF to optimize the wave reflection solutions. In addition, several parameters are analysed in order to optimize the solutions. The developed numerical model and its key findings are compared with analytical and experimental surface elevation results and it reveals a good correlation. Finally, the recommended numerical solutions are validated with the experimental findings.

Keywords: breakwater; CFD; numerical wave flume; scattering coefficients

1. Introduction

In the design and the execution of marine structure, it is paramount important to understand the fluid/structure interaction. In the past, physical model studied are carried out in a wave flume or wave basin, on a scale model in real sea conditions. However, with the recent developments in computational fluid dynamics (CFD) software and open-source tool now it is possible to carry out time efficient and relatively initial studies by numerical approach. The outcome of such studies is used to represent of the real-life environment. Keeping the rough sea conditions in mind, the coastal structures have to meet several criteria before installation and execution. These structures must be rigid and flexible, highly resistant to corrosion, allow for maintenance interventions, and withstand severe conditions such as storms and many other aspects. On the other hand, several investigators have worked on developing numerical wave flumes for simulating ocean waves and reproducing the physical condition accurately. Several investigators have used analytical codes to generate ocean waves in an NWF. (Lal and Elangovan 2008, Kumaran *et al*. 2021, Liang *et al*. 2010, Vijay *et al.* 2021). Fatemeh *et al*. (2007) developed a RANS equation - VoF method-based numerical model to investigate the wave breaking, the resultant local velocity, turbulence, and overtopping over the breakwater. Silva *et al*. (2010) provide accurate results in the simulations and generation of regular waves in the water depths ranges of ($d/L \leq 20$). The key findings are compared with analytical formulations and also studied the significance of the domain height, convergence of mesh & time

*Corresponding author, Dr., E-mail: vkumaranms@gmail.com

http://www.techno-press.org/?journal=ose&subpage=7 ISSN: 2093-6702 (Print), 2093-677X (Online)

discretization on the water surface elevation (η). Finnegan and Goggins (2012) investigated the linear deep-water waves using the ANSYS CFX tool. Several tests are performed to see the influence of various parameters on the waves generated, including the computational grid size, domain length and height, time step interval, and beach slopes. The outcomes show excellent correlations in comparison with the linear wave theory. In a physical model study, the wave reflection is analysed by various methods available in the literature (Goda Suzuki 1972, Mansard and Funke 1980, Zhu 1999, Isaacson 1991). Maguire *et al*. (2011) studied various beach slopes and recommended a slope value greater than 1:10. Similarly, Fabio *et al*. (2018) and Finnegan *et al*. (2012) investigated slopes 1:3 to 1:6, and both works concluded that 1:5 is the ideal slope condition. Elangovan (2011) investigated the effect of beach slope on wave reflection and concluded that a beach slope of 1:3 is better in reducing wave reflection. Kamath (2012) investigated several grid cell densities, and each wavelength starts with a minimum of 10 grid cells. When the density of grid cells is small, the wave's amplitude is significantly reduced as it propagates through the NWF because of the numerical diffusion. Mohammed *et al*. (2016) numerically studied the hydrodynamic performance of two types of innovative breakwaters with two vertical perforated walls, of different permeabilities, with and without, horizontal slotted walls in between and validated them with results from experimental studies. Zheng *et al*. (2016) studied the wave structure interaction using open foam to simulate the wide range of non-linear wave conditions. Tian *et al*. (2018) investigated the effect of the wave interaction with a vertical cylinder in a 3-Dimensional numerical wave flume and compared the results with analytical solutions. They observed that Fluent code could accurately model the generation of regular waves. Nizamani *et al.* (2021) investigated the stress imposed on offshore structures by environmental factors using CFD and concluded that inaccuracy is less than 3% for maximum lifting force whereas an inaccuracy of 15% was observed during the minimum lifting force. Kumaran *et al*. (2022) implemented the numerical wave flume to access the performances of a slotted barrier. The outcome of the study aid in designing coastal structures for the actual wave conditions. Kandula *et al*. (2022) studied the cavitating effects of fluid flow past different axisymmetric activator in a water tunnel experimental study and a numerical model (CFD- Fluent) is developed and validated the same with the experimental findings. Chang *et al*. (2018) studied the bragg resonances by cnoidal and stokes waves wave theory and in the numerical results exhibit higher resolution for examining the secondary eddies com-pared with the conventional numerical methods. Priya *et al*. (2000) studied the hydraulic parameters such as wave reflection, transmission characteristics, hydrodynamic pressures and forces on a submerged semi-circular breakwater model and the hydrodynamic pressures are compared with the 2-D finite element model of Sundar *et al.* (2000) and good correlation is observed. Chen *et al*. (2019) observed the effective reduction in the propagation of spurious-free harmonic waves based on the numerical model of the second-order wave-maker theory. In Spatio-temporal domains, a stable wave profile can be created based on this model. Similarly, the FFT techniques are also used to analyse all the amplitudes of Fourier components from two simultaneous wave recordings taken at adjacent locations, which can be applied to both regular and irregular wave trains. Yuan and Tao (2003) investigated the wave force acting on SBWs under submerged and emerged conditions. The numerical solutions based on the hybrid method of the BEM and the finite difference method and fluid motion described by the velocity potential are used to study the wave force on SBW. The numerical solutions are validated with five sets of experimental data of semi-circular breakwaters and good correlations are obtained between the numerical and experimental results.

Keeping these motives in mind and significantly reducing wave reflection in a numerical wave flume, an extensive work i.e., varying the mesh size, beach slope and NWT length is carried out on

ANSYS-Fluent computational fluid dynamics based on the RANS equations. The computational results are validated with the results obtained from a theoretical (stokes equations) and experimental result of Binomol *et al.* (2017). The outline of the research work is as follows. The theoretical model, the numerical governing equations using ANSYS-FLUENT, and meshing details for the computation domain are discussed in Sections 2 & 3. Section 4 elaborates on the physical model setup in the wave flume facility at Central Water & Power Research Station (CWPRS)- Pune, India. Section 5 focuses on the various interpretation of results for understanding the effect of beach slopes, and finally, the validation of recommended NWF is highlighted with the performance of QCB.

2. Theoretical method

2.1 Stokes wave theory

Stokes wave theory, a nonlinear one, describes regular finite amplitude progressive waves. Real waves have shorter crests and deeper troughs, while sinusoidal waves have the same height and length of crests and troughs, respectively. The equation in the dimensional form of Laplace is given in Eq. (1). At the same time, the wave steepness H_i/L is small but not infinitely small as for regular waves. This assumption is reasonable since, in actual waves, the steepness never exceeds 0.10-0.15.

$$\nabla^2 \emptyset = \frac{\partial^2 \emptyset}{\partial x^2} + \frac{\partial^2 \emptyset}{\partial x^2} = \emptyset_{xx} + \emptyset_{zz} = 0 \tag{1}$$

The boundary conditions to be satisfied are the free surface kinetic boundary condition

$$\emptyset_z = 0; \qquad z = -h \tag{2}$$

$$\eta_t \; 0 + \; \emptyset_x \eta_x - \emptyset_z = 0 \quad ; \; z = -\eta \tag{3}$$

$$\eta + \frac{1}{2g}(\; \emptyset_x^2 + \emptyset_z^2) + \; \frac{1}{g}\emptyset_t = \frac{C(t)}{g} \quad ; \; z = \; \eta \tag{4}$$

Where C(t) is the arbitrary function in the generalized Bernoulli equation.

In addition, we assume the waves are periodic in x, which we express as

$$\emptyset_x(0, z, t) = \emptyset_x(L, z, t) = 0 \tag{5}$$

The dimensional form of the equations and solutions are based on the assumption that if we define the parameter γ as

$$\gamma = \delta\epsilon = \frac{H}{h}\frac{h}{L} = \frac{H}{L} \tag{6}$$

Then we have nonlinear terms = O(γ). Linear terms.

$$\eta = a\cos\theta + \frac{\pi}{L}a^2 f_2\left(\frac{d}{L}\right)\cos 2\theta + \left(\frac{\pi}{L}\right)^2 a^3 f_3\left(\frac{d}{L}\right)\cos 3\theta \tag{7}$$

Eq. (1) gives the free surface elevation (η) of the wave according to Stokes third-order theory. Where a = amplitude of the wave for the first-order term in the expression of surface elevation, d= water depth (m), L= wavelength (m).

$$f_2\left(\frac{d}{L}\right) = \frac{cosh\frac{2\pi d}{L}(cosh\frac{4\pi d}{L}+2)}{2(sinh\frac{2\pi d}{L})^3} \tag{8}$$

$$f_3\left(\frac{d}{L}\right) = \frac{3}{16}.\frac{8\,(cosh\frac{2\pi d}{L})^6+1}{(sinh\frac{2\pi d}{L})^6} \tag{9}$$

In the third-order approximation, the Eq. (7) can be written as

$$\eta = a_1 \cos\theta + a_2 \cos 2\theta + a_3 \cos 3\theta \tag{10}$$

And finally, the stokes higher-order expressed in Eq. (8)

$$c^2 = \frac{gL}{2\pi} tanh\frac{2\pi d}{L}\{1 + (\frac{2\pi a}{L})^2 \frac{cosh\frac{8\pi d}{L}+8}{8(sinh\frac{2\pi d}{L})^4}\} \tag{11}$$

The Eq. (11) (stokes higher-order) waves have dispersive frequency and amplitude.

3. Numerical method

3.1 Governing equations

To solve the incompressible N-S equations for two-phase flow (air, water) and for tracking the free surface in the numerical computational setup Volume of Fluid (VOF) scheme is incorporated (Viswanathan *et al.* 2021). Finite-volume based numerical model solves the governing equations.

3.1.1 Equation of continuity

Given when the equation for conservation of mass is coupled with the assumption of incompressibility

$$\frac{\partial u}{\partial x} + \frac{\partial v}{\partial y} = 0 \tag{12}$$

Where, u-x velocity components (m/s)
v-y are the velocity component (m/s)

3.1.2 Navier stokes equation

Obtained using the equation of continuity with conservation of momentum, written as

$$\rho\left(\frac{\partial u}{\partial t} + u\frac{\partial u}{\partial x} + v\frac{\partial u}{\partial y} + w\frac{\partial u}{\partial z}\right) = -\frac{\partial p}{\partial x} + \mu\ \left(\frac{\partial^2 u}{\partial x^2} + \frac{\partial^2 u}{\partial y^2} + \frac{\partial^2 u}{\partial z^2}\right) + \rho g x \tag{13}$$

$$\rho\left(\frac{\partial v}{\partial t} + u\frac{\partial v}{\partial x} + v\frac{\partial v}{\partial y} + w\frac{\partial v}{\partial z}\right) = -\frac{\partial p}{\partial y} + \mu\ \left(\frac{\partial^2 v}{\partial x^2} + \frac{\partial^2 v}{\partial y^2} + \frac{\partial^2 v}{\partial z^2}\right) + \rho g y \tag{14}$$

Where *u and v* are the velocity components along the *x and y* axes, respectively (m/s), ρ is density (kg/m^3), μ is dynamic fluid viscosity, p is pressure (Pa), g is the acceleration of gravity (m/s^2), and t is time (s).

Either implicit or explicit discretization of time can be used to solve the volume fraction equation (Ansys manual 2020). In describing free surface and nonlinear wave motion, Navier-Stokes equations (Eqs. (13) and (14)) and continuity equations (Eq. (12)) are used. The water density remains constant (i.e., incompressible) and follows Newton's law of viscosity. A schematic representation of the numerical wave flume model is illustrated in Fig. 1.

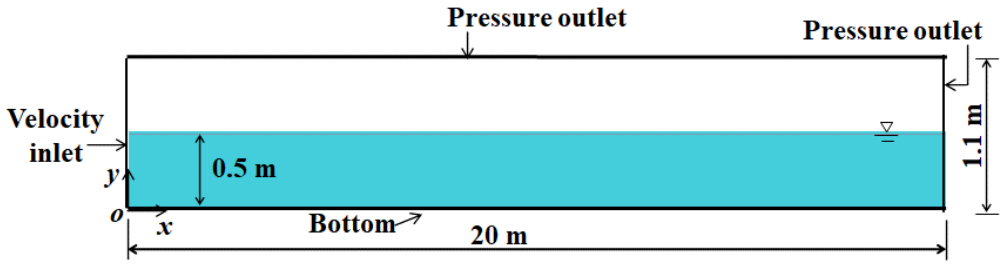

Fig. 1 Numerical Wave flume model

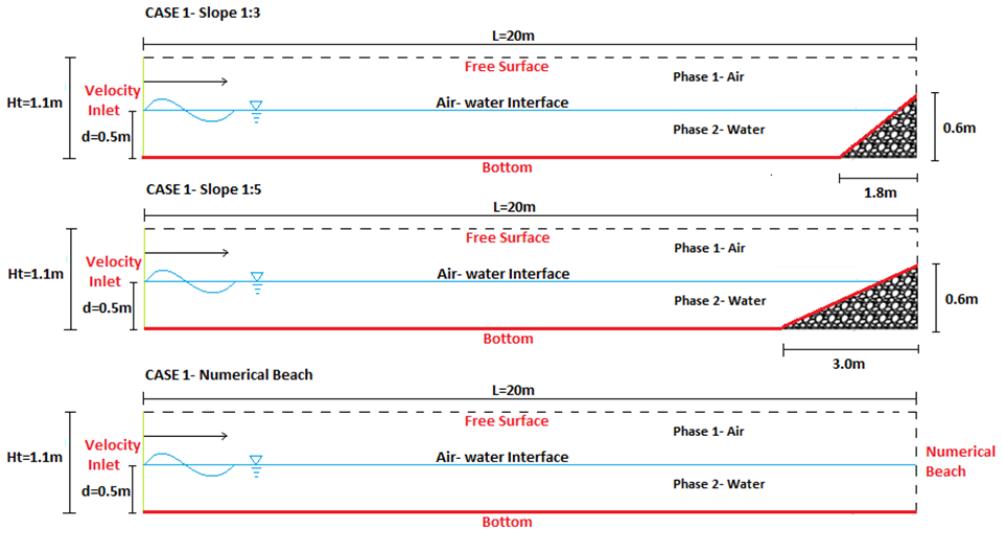

Fig. 2 Schematic NWF with boundary conditions and varying beach slopes (not to scale)

3.2 Modelling of geometry

A 2-D NWF geometrical model has a length of 20 m, and a height of 1.1 m with a 0.5 m water depth, and the NWF length is chosen to be twice the wavelength (L) of the maximum L considered in the study. It is enough to generate a fully matured wave to capture the proper wave-structure interaction. So that the wave-making area is not influenced by wave reflection from the downstream end. (length of NWF as 20 m (>12 m)), and the height of NWF is kept the same as the experimental setup. The geometrical model is designed by the Ansys design modeller tool. The geometry for numerical simulations with varying beach slopes with boundary conditions is illustrated in Fig. 2. Similarly, the slope characteristics are tabulated in Table 1. The parameters considered for optimization are three different sizes of mesh i.e., 0.01 m x 0.01 m. 0.02 m x 0.02 m and 0.03 m x 0.03 m, varying end slopes (1:3, 1:5, Numerical beach) and Numerical tank length (20 m, 30 m, 40 m) are discusses in the sub-sequent sections.

Table 1 Slope Characteristics

Slope Characteristics	Case 1- Slope 1:3	Case 2- Slope 1:5	Case 3- Numerical Beach
V	0.6 m	0.6 m	-
H	1.8m	3.0 m	-

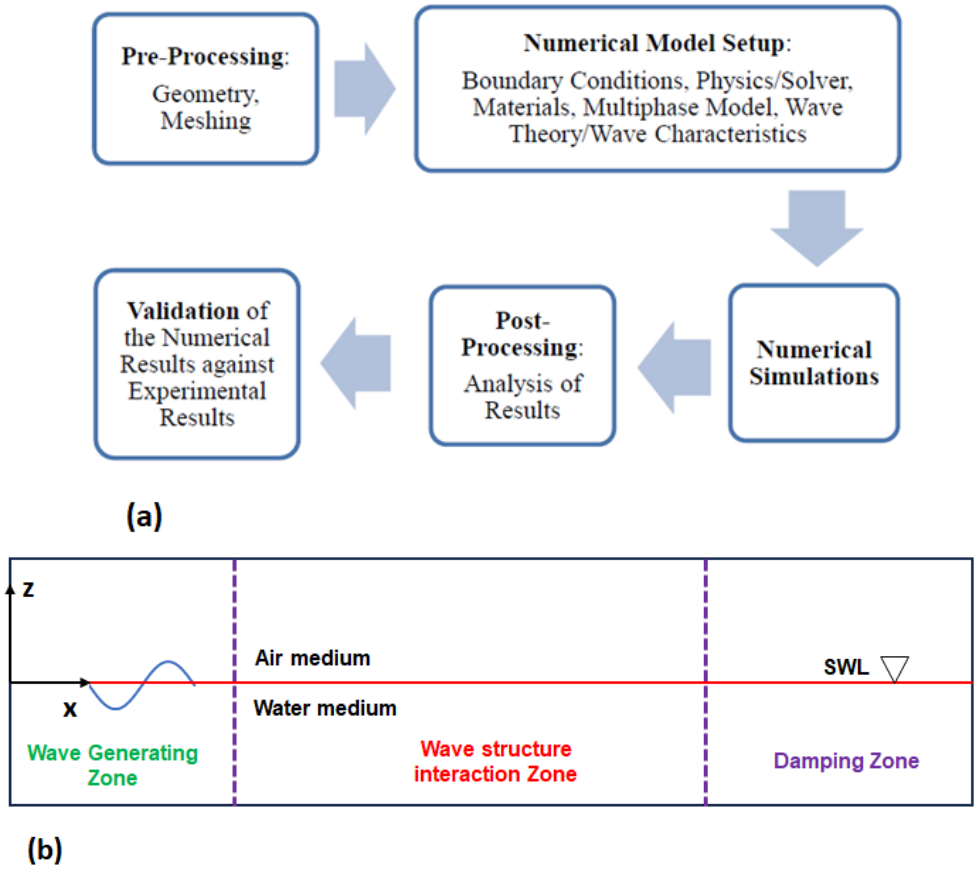

Fig. 3 Workflow & different zones in Numerical Simulations Ansys-Fluent

In the present numerical computations, a numerical beach is put at the end of NWT. As the absorbing technique, are considered by the method proposed by Cointe *et al*. (1990) where proper damping is added to free-surface conditions. On side walls, we don't impose any numerical beach technique and allow of wave reflections. A sloping beach (1:3 & 1:5) is considered similar to verify what happens in real beach. Sloping beach has the merit of investigating wave breaking on slope.

The general steps involved in numerical simulation of ANSYS - FLUENT can be broadly classified into three. Pre-processing, Solver, and Post-processing. Pre-processing can be subdivided

Table 2 Grids Parameters

Meshing Details	Δx (m)	Δz (m)	Grid Cell Density	No. of Elements	No. of Nodes
1.	0.03	0.03	200	24076	24775
2.	**0.02**	**0.02**	**300**	**55742**	**56796**
3.	0.01	0.01	600	220008	222119

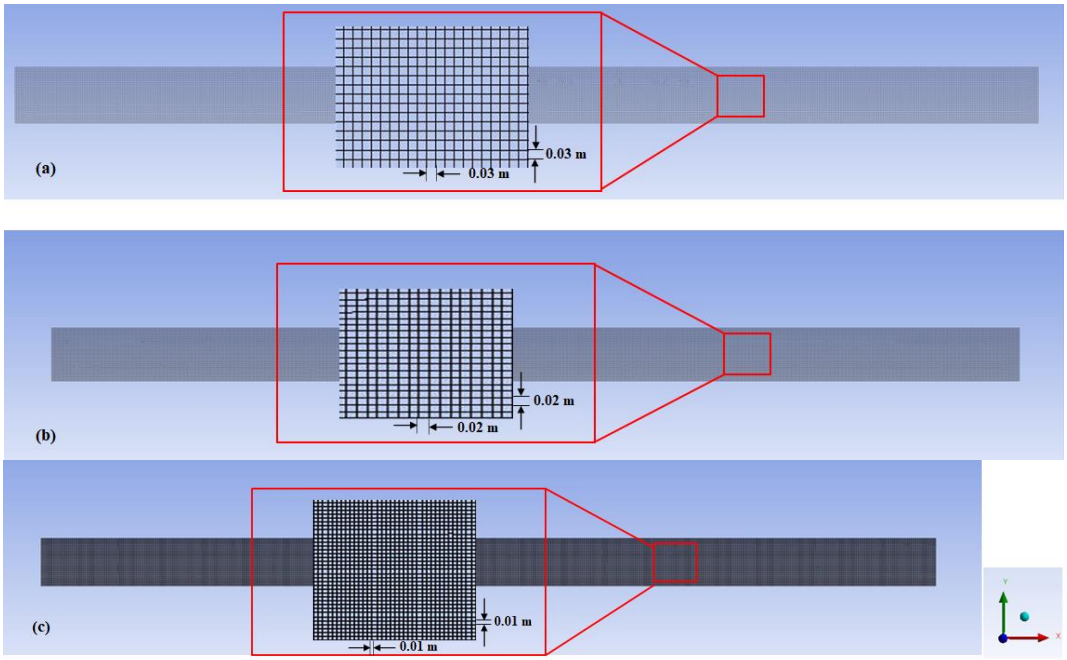

Fig. 4(a)-(c) Fluent meshing closer to the test model

into Geometry building, Meshing, and defining the boundary conditions, as illustrated in Figs. 3(a) and 3(b) highlights the different zones i.e., wave generating zone, working zone & damping zone for the computational domain.

3.3 Meshing details

The suitable mesh selection determines the solution's accuracy, stability, and computational efficiency. Hence in this segment, we devote a detailed discussion on the grid size or mesh details. The numerical grid pattern is created using the Ansys mesh tool. Using the face meshing method, the solution region is divided into square elements of chosen dimensions, and then a structured mesh is created. Initially, to determine the effect of mesh size on the accuracy of ANSYS Fluent results, a two–dimensional Numerical Wave Tank is modelled, and the wave surface elevations are obtained. The computational simulations are carried out for three mesh sizes, viz. 0.01 m x 0.01 m. 0.02 m x 0.02 m and 0.03 m x 0.03 m as shown in Figs. 4(a)-4(c). Table 2 shows the base grid dimensions for which the trials are carried out. Havn (2011) recommended the criteria for sizing the mesh and time step for better accuracy. The mesh size parameters are illustrated in Table 2.

Table 3 Mesh convergence study

Mesh size	0.01 m	0.02 m	0.03 m
Incident Wave Height (m)	0.10	0.10	0.11
	0.12	0.12	0.13
	0.14	0.14	0.16

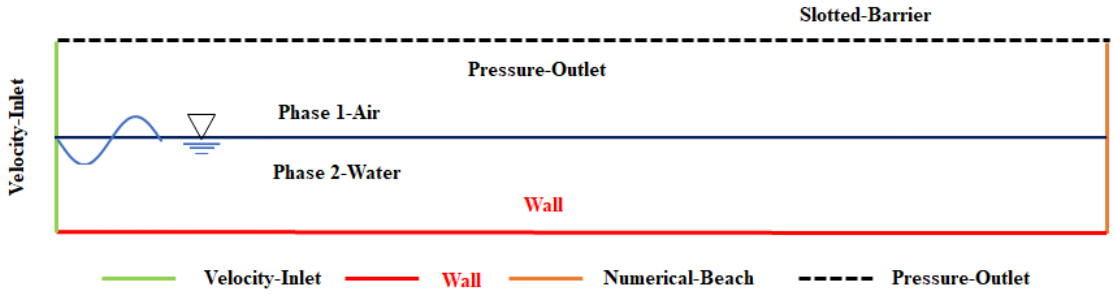

Fig. 5 Boundary conditions

From the mesh convergence results obtained for the cases mentioned above, inferences are drawn that higher grid cell density gives more accurate results. But the computational time is very high than the same. So, it can be inferences that higher grid cell density is preferred for more accurate results while increasing the nodes and elements in the computation domain with finer mesh results more in time. But from the mesh convergence study shown in Table 3, the grid size of 0.02 m is observed with similar trends compared with the 0.01 m grid size. Hence, for the present study, the NWF meshes into structured square meshes of 0.02 m grid size, and the whole structure meshes uniformly into a square structured mesh of 0.02 m x 0.02. Due to that, the computational time reduces as fewer elements are used. Meanwhile, varying the beach slope at the downstream end of NWF doesn't significantly affect mesh size.

3.4 Boundary conditions

As we solve the 2nd order governing equation in 2-D, we need four boundary conditions to get the solution mathematically. Here in the physical domain, we have the following four boundary conditions.

(i) Inlet = velocity inlet
(ii) Oulet = pressure outlet
(iii) Bottom = wall (no-slip condition)
(iv) Top = free surface

The boundary conditions are illustrated schematically in Fig. 5.

The NWF involves multiple phases, i.e., air and water. Flowing media (water) is always set as the secondary phase, and the medium over that is a primary phase (air). Fluent automatically assumes that the preliminary phase species is present in every cell unless otherwise mentioned. Creating the secondary phase (water) within the domain is assigned over the required portion to provide a constant fill level equal to the chosen water depth (d=0.5 m). For clarity, the actual boundary

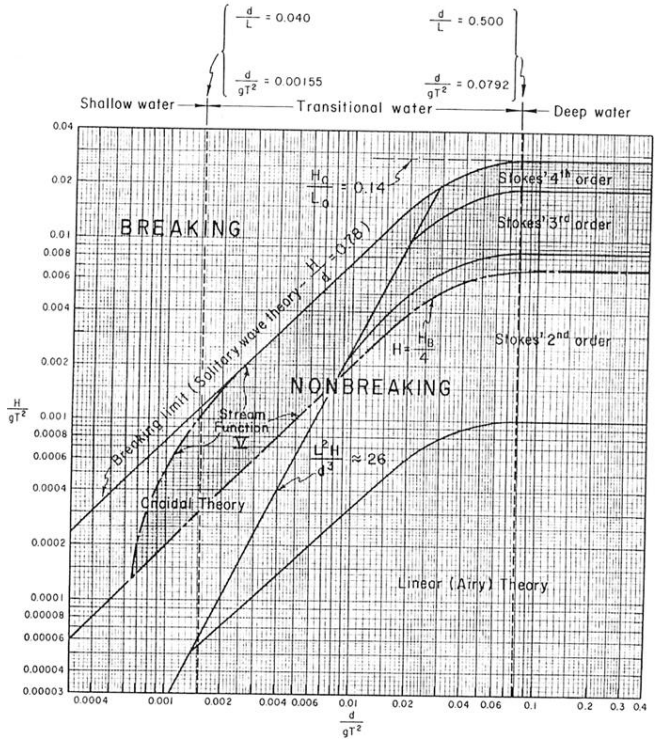

Fig. 6 Ranges of validity for various wave theories (Le Mehaute 1969)

conditions are shown in Fig. 5. The ocean wave is generated using a User Defined Function (UDF) to the inlet velocity boundary within the Fluent analysis module. A unique UDF is created for each water depth (d), wavelength (L), wave height (H), and wave period (T) combination.

As an initial condition, static pressure is given for the liquid face, and the free surface between the air and water interface is generated by the volume of the fluid model (VOF). The implicit formulation is used for the volume fraction parameter.

The numerical simulations are frameworks with two-phase air and water, having a constant density of 998 kg/m^3 for water and 1.225 kg/m^3 for air. The turbulence model chosen is a standard k-ε viscous model. To simulate the wave condition, the wave theory is selected based on Chakrabarti (1987), wherein the analysis involves the wave conditions from ($1/20 \leq d/L \leq 1/2$) shown in Fig. 6.

4. Experimental method

4.1 Wave flume set-up

The physical model studies are conducted in the wave flume facility at Central Water & Power Research Station (CWPRS)- Pune, India (Fig. 7). The wave flume has the following dimensions: Length = 50 m, Height = 1.8 m, and Breadth = 1.2 m. An electronically powered flap-type wave

Fig. 7 (a) Flap type paddle, (b) Flap type paddle, (c) Frequency drive and (d) Lengthwise wave flume

generator is equipped in the wave flume. It is capable of generating regular waves. An active wave absorption system is provided in the downstream end for controlling the reflected wave.

The surface elevations are determined by measuring the wave parameter at different locations by placing the capacitance-type wave probes inside the flume. The wave probes are 0.5 m long with a resolution of 0.02 mm, and the tolerance of error is +/- 1%. The calibration of wave probes is done before conducting the physical model study.

4.2 Experimental setup

The experimental section is placed at halfway of the wave flume, which is 28 m from the wave generation zone. The experimental wave flow phenomenon is observed through the glasses attached along one side of the wave flume. The wave recorder or synthesizer software has the flexibility to select any combinations of regular waves (H, T). The signal for the wave motion from the flap-type paddle is generated by a computer. The wave probes WP1, WP2, and WP3 measure the waves influenced by the incident waves. The experimental runs are collected for 30 s, and validation 15sec data are used. An artist view showing the wave flume setup and positions of wave probe arrangements are shown in Fig. 8.

The primary input parameters:

- Incident wave height, H_i
- Wave period, T
- Water depth, d (d=0.5 m)
- The wavelength, L

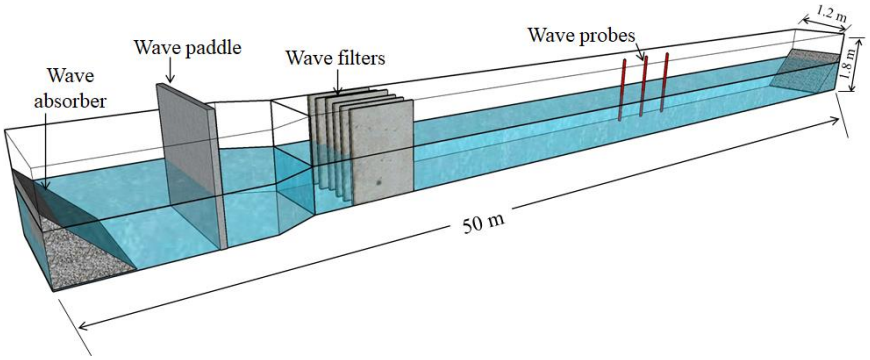

Fig. 8 Artist view of the experimental arrangement

5. Results and discussion

Here, we are discussing the various effects of beach slopes (1:3, 1:5, and a numerical beach state) in reducing the wave reflection characteristics, and the validation of the numerical model is done by comparing it with an experimental and theoretical approach. The outcomes of 2D computational results apply to extensive wave conditions. The following input parameters remain fixed throughout the study, such as the water depth (d = 0.5 m) and NWF wave theory unless otherwise mentioned.

5.1 Influence of beach slope

Various researchers have investigated several methods and techniques to dissipate the wave attenuation at the downstream end of the NWF (Maguire 2011, Fatemeh 2007, Neves 2021). Wang *et al.* (2020) investigated the comparison study of the three major types of phase-resolved wave models and the differences among those wave models. In the present study, the NWF is tested in a water depth of 0.50 m with varying wave heights (0.12 m to 0.18 m) and wave periods (1.4 s and 2.8 s). Two beach slopes (1:3 & 1:5) and numerical beach conditions are employed to dampen the wave energy and investigate optimum beach slopes for NWF. The measured wave elevations for different beach slopes at 3m from the end of the beach are shown in Fig. 9. A 3m is chosen from the downstream end of the beach to avoid the nonlinearities resulting from the wave breaking. The beach slope of 1:5 is optimum as the difference in the degree of wave damping, and the phase shift is insignificant compared to a slope of 1:3. Further, Fig. 9 shows the free surface elevations of the fully matured wave and the dissipated wave near the downstream end of the numerical beach. It is observed that the sloping beach effectively dampens the wave compared to numerical beach conditions. A minimum slope needed for preventing the reflected wave the different slopes were considered and the surface elevation (η) wave horizontal velocity are monitored. The results showed that within the range of this paper, a minimum slope of 1:5 is sufficient to avoid wave reflection in fluid domain.

5.2 Analysis of errors

The error analysis is performed to check the significance of the developed numerical model. The key factors affecting the wave generation are analysed, considering the cells and the number of

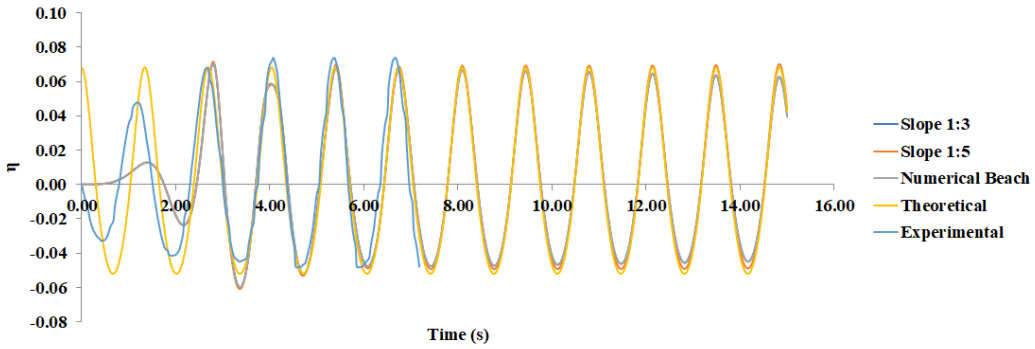

Fig. 9 η v/s t graphs for comparison of numerical, theoretical & experimental results (For H=0.12 m, T=1.4s)

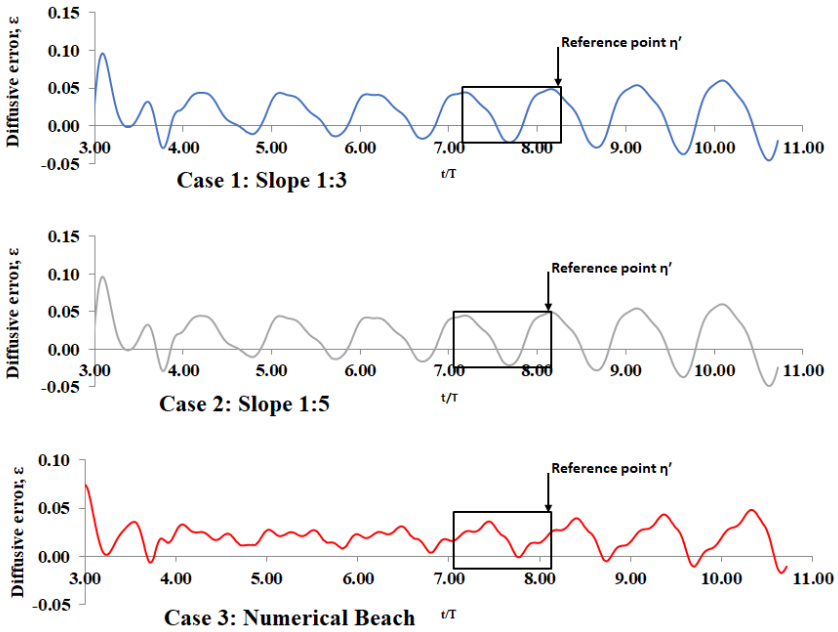

Fig. 10 Diffusive Error v/s t/T (For H=0.12 m, T=1.4s)

points per wave height. The theoretical solutions are used as the reference solution. A regular wave with the wave period T = 1.4 s and wave height H = 0.12 m at a water depth of d = 0.5 m is propagated in the numerical wave flume for 15 wave seconds. In each wave period, a uniform distribution of 10 points was used to calculate the diffusive error using.

In each case, the diffusive error, ε, was calculated using

$$\varepsilon = \frac{1}{H}(\eta - \eta') \tag{16}$$

Where η and η` denote the numerically computed free-surface elevation and the reference point elevations (Zhang *et al*. 2019), the results obtained in the NWF after about the initial 4 seconds of simulation are used for the analysis to avoid any spurious results at the beginning of the test. The variations of diffusive error with time normalized by the wave period for (t/T) = (0.12 m, 1.4s) are plotted as follows in Fig. 10.

The relative error is calculated by taking the analytical solution and reference point as reference. As evident from the graphs, in all three cases, it can observe that the error through all the domain lengths is minimal. The maximum diffusive error for slope 1:3 (Case 1), 1:5 (Case 2), and numerical beach (Case 3) are 5.2 %, 4 %, and 4.5 %, respectively, all of which are within the acceptable limit. (Oberkampf and Blottner 1997).

5.3 Influence of the numerical wave flume length

Numerical simulations are carried out for different wave tank lengths L (20 m, 30 m, 40 m). The comparison plots are illustrated in Fig. 11. The water surface elevation at t=15 s for different tank lengths is noted that a reduction in the length of the NWF to 20 m causes the reflection of the waves to affect the surface elevation at the downstream end and a shift in nature. At the same time, increasing the NWF length to 30 and 40 m does not show any improvements, but it results in higher simulation time for conditions considered in the present study, in case of theoretical value slight variations observed within the acceptable limit.

Increasing the tank length is an effective solution to prevent wave reflection; on the other hand, a 20 m wave tank (twice the maximum wavelength consider in the study) gives better results.

5.4 Validation of the NWF against experimental results

To validate the results from NWF against the experimental results, the time series of free surface elevations for all the cases from the numerical procedure is plotted. A comparison with experimental results is illustrated in Fig. 12.

A UDF is defined for the components of inlet velocity to generate ocean waves numerically to simulate the wave theory. This numerical wave flume gave considerably good results in-line with the experimental results. For the time step of 0.01 s (T/200), surface elevation in the wave crest and

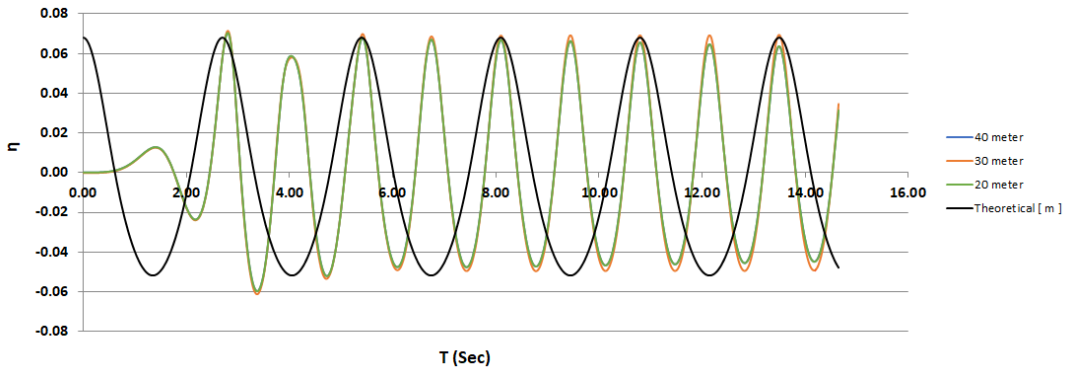

Fig. 11 η v/s t graphs for comparison of various tank lengths & theoretical results (For H=0.12 m, T=1.4s)

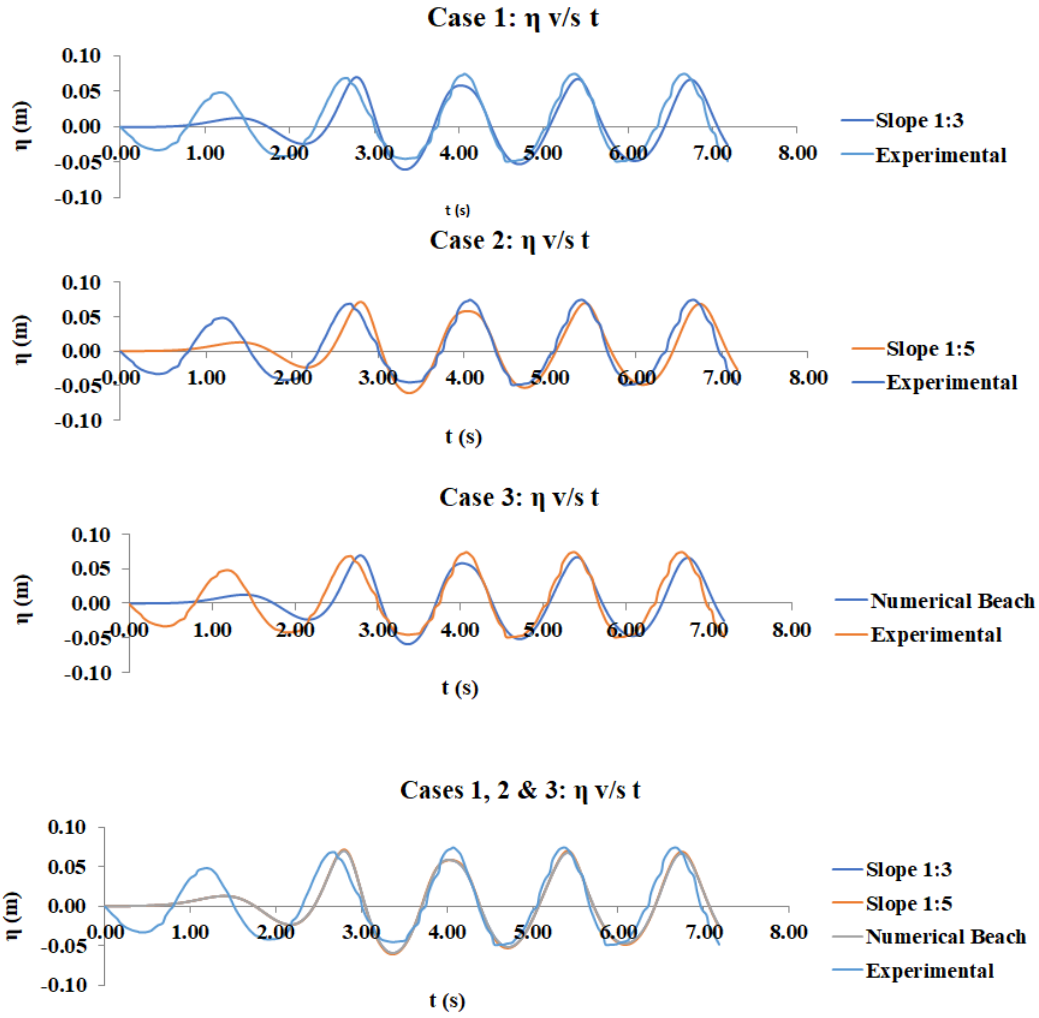

Fig. 12 Comparison of η v/s t plots for different NWF with experimental results (For H=0.12 m, T=1.4s)

trough obtained from the numerical study closely correlates with the analytical study. Hence the time step of 0.01 s is considered for all CFD simulations.

5.5 Validation of recommended parametric solutions with experimental findings

5.5.1 Comparison of wave profile obtained from the recommended NWF with experimental results

The comparison of the wave surface elevations (η) between the experimental results and the simulated results for a case of H_i/d=0.24, T = 1.4 s with the recommended mesh size of 0.02 m x 0.02 m, with a timestep of 0.01 s, 20 m tank length and numerical beach condition is illustrated in Fig. 14. The discrepancies in the wave height and phase for a few waves are observed owing to the

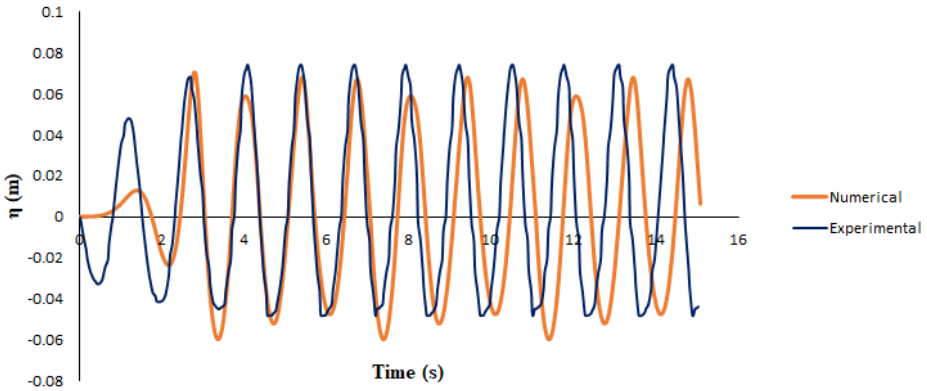

Fig. 13 Variation of free surface elevation (η) between experimental and computational results; Relative Wave height (H_i/d) =0.24, Wave period (T)=1.4 s

fact that the numerical dissipation in the simulation might affect the wave behavior, causing damping or alterations that are not present in the physical experiments. But a general agreement between the numerical results and the experimental results is reasonable. The relative error is used to analyse the numerical and experimental results are quantitative.

$$\text{Relative error} = \frac{Ep - Np}{Ep} \times 100$$

Where E_p - Experimental results

N_p - Numerical results

The mean relative error in wave height measured by the wave probe is 3.8 %, and the free surface elevation variation shows good correlations between experimental study and numerical solutions.

5.5.2 Validation of recommended NWF with the hydraulic parameters of a quarter circle breakwater

The recommended parametric solutions are validated by the experimental findings of Binumol *et al*. (2017), on the performance of quarter circle breakwater. The depth of NWF (1.1 m) is fixed the same as the physical wave flume at NITK, Surathkal. The test conditions and wave characteristics are illustrated in Table 4.

5.5.3 Computational domain (Meshing details)

The computational mesh is created using the Fluent Meshing tool. The face meshing method is used to create a structured mesh, in which the domain is divided into square elements of specified dimensions. The relatively simple geometry of the NWT allows for efficient modelling of the domain using quadrilateral cells. The base grid dimension of 0.02 m x 0.02 m is chosen which provides in the order of 300 cells per wavelength for typical test conditions, which are finer and more accurate than, a minimum grid cell density of 200. (Kamath 2012). The selection of grid size is elaborated in the earlier section 3.3. Fig. 14, shows the computational mesh of QCB in a numerical wave flume and the boundary conditions are illustrated in Fig. 15.

Table 4 Range of wave parameters used for validation of NWF

Parameters	Range of Values
Water depth, d (m)	0.35-0.45
Incident wave height, Hi (m)	0.03 - 0.18
Wave period, T (s)	1.2 - 2.2
Radius of QCB,R (m)	0.55

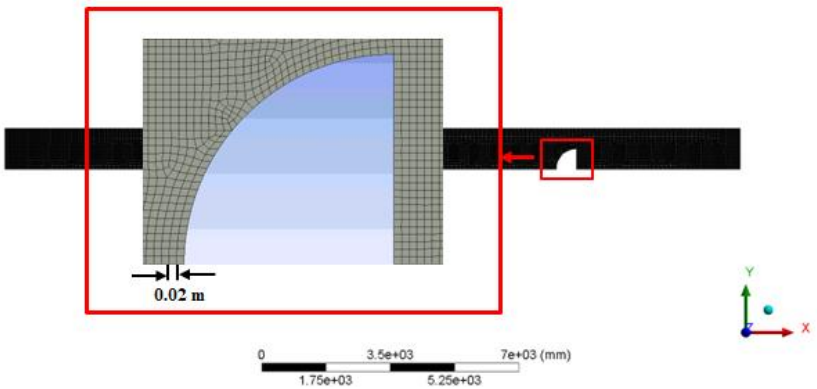

Fig. 14 Generated mesh model for test model (QCB - 0.02 m x 0.02 m)

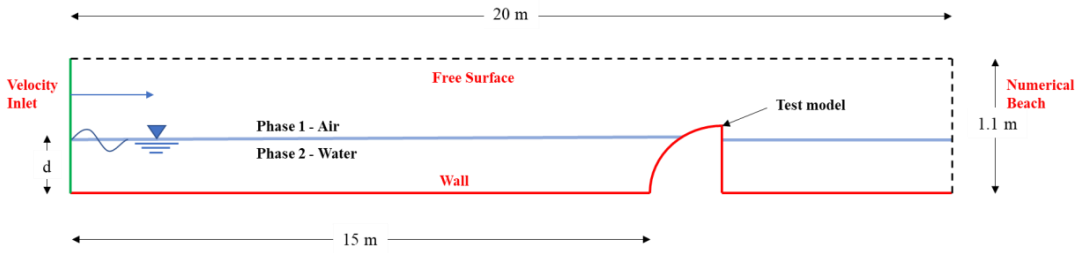

Fig. 15 NWF with boundary conditions

5.5.4 Boundary conditions

In the previous section 3.4, a detailed discussion is given regarding the boundary conditions. The same conditions are adopted while implementing the test model of QCB in a numerical wave flume.

5.5.5 Comparison of the numerical and experimental wave reflection coefficient (K_r)

Fig. 16, show the validation of Kr with H_i/L for different d/hs. For the quarter circle breakwater, the minimum K_r value of 0.479 is observed at d/hs equal to 0.732 (0.45 m water depth) and the maximum K_r obtained is 0.823 when d/hs equal to 0.569 (0.35 m water depth). For quarter circle

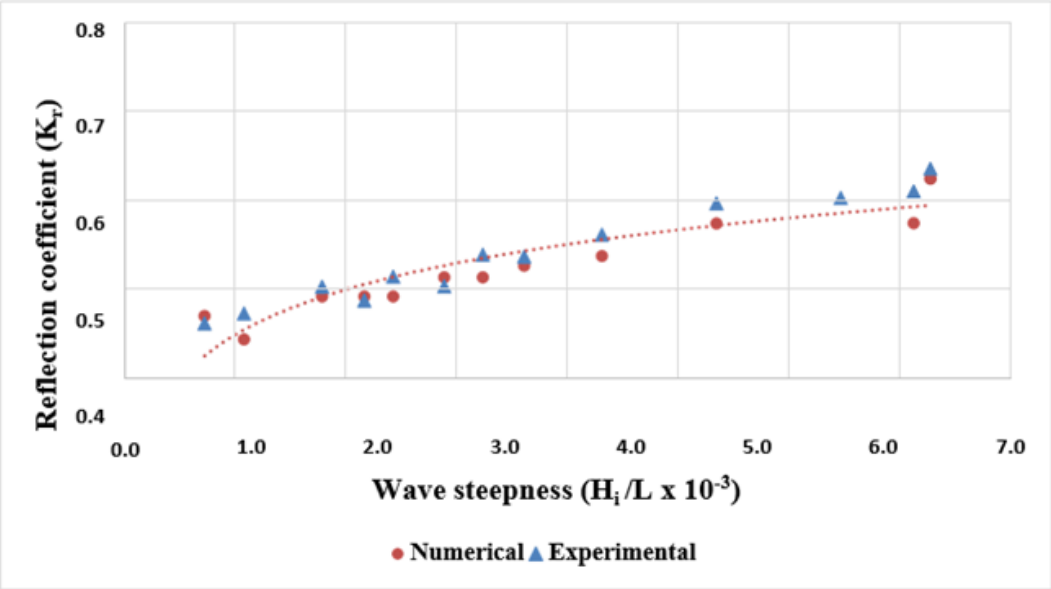

Fig. 16 Comparison of numerical and experimental wave reflection coefficient (K_r) with Wave steepness (H_i/L), for d/hs = 0.732

breakwater of radius 0.55 m (h_S = 0.615 m), K_r varies from 0.479 to 0.660 for 6.318 x10^{-4}< H_i/L < 6.3710 x10^{-3}. The minimum K_r observed is 0.479 at a wave height of 0.03 m and awave period of 1.8s (H_i/L= 9.439 x10^{-4}) and a water depth equal to 0.45 m (d/h_S = 0.732).

On comparing, the numerical and experimental K_r values from the above Fig. 20, it is noticed that the experimental and numerical Kr values are in good correlation with a minimum deviation of 1.431% and a maximum deviation of 6.64%. The deviations are found to be well within the acceptable limit. Using the error analysis equation as discussed in section 6.2.

5.5.6 Comparison of the numerical and experimental Relative Wave Runup (R_u/H_i)

The wave runup (R_u/H_i) is the vertical height reached by the up-rushing wave above the still water level (SWL). The wave runup on QBW is usually expressed in terms of relative wave runup, R_u/H_i which is an essential parameter for fixing the crest elevation for non-overtopping conditions and it mainly depends on water depth, and structure parameters like breakwater radius and wave parameters. The results obtained from the numerical studies are plotted as non-dimensional graphs showing the variation of relative wave runup with wave steepness, (H_i/L) for different relative water depths, and d/hs. Fig. 17, shows the comparison plots of relative runup (R_u/H_i) with wave steepness (H_i/L).

The minimum (R_u/H_i) observed is 1.753 at a wave height of 0.09 m and a wave period of 1.2s ((H_i/L) = 6.371x10-3) and at 0.45 m water depth (d/hs = 0.732). Further, from Fig. 20, it is observed that (R_u/H_i) decreases with an increase in depth. The higher the water depths, the effect of curvature is more pronounced, and this results in a lower runup. In comparison of values obtained by experimental results to the values from the present study, the percentage error is in the range of 1.90% to 6.36% which is within the acceptable limit.

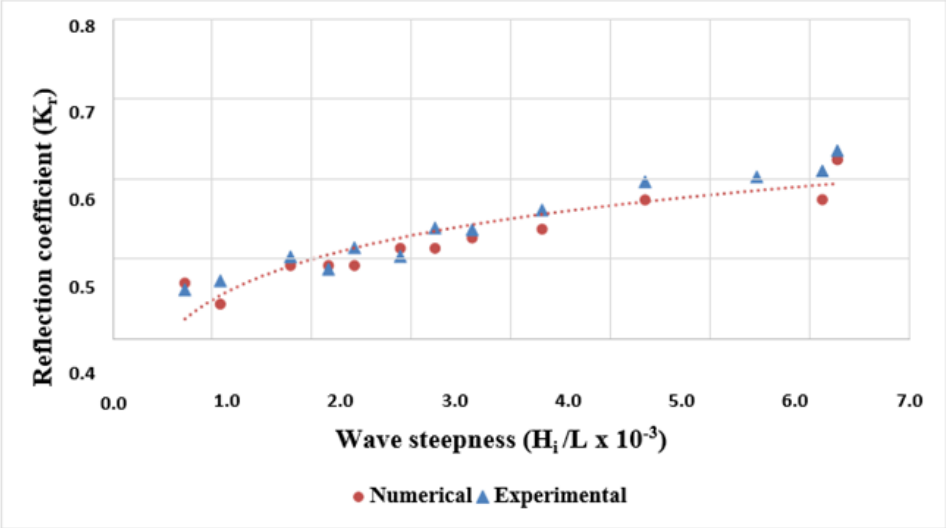

Fig. 17 Comparison of numerical and experimental relative wave runup (R_u/H_i) with Wave steepness (H_i/L), for d/hs = 0.732

5.5.7 Comparison of the numerical and experimental loss coefficient (K_l)

Fig. 18, demonstrates the variation of numerically determined loss coefficient (K_l) as a function of wave steepness (H_i/L) for a water depth of 0.45 m for a quarter circle breakwater. For QBW of radius equal to 0.55 m (hs equal to 0.615 m), K_l varies from 0.751 to 0.877 for 6.318x10-4 < H_i/L <6.3710x10-3. The maximum K_l observed is 0.877 at a wave height of 0.03 m and a wave period of 1.8s (H_i/L = 9.439 x10-4) and water depth equal to 0.45 m (d/hs = 0.732). The loss coefficient, K_l decreases with an increase in H_i/L and also decreases with an increase in hs/d.

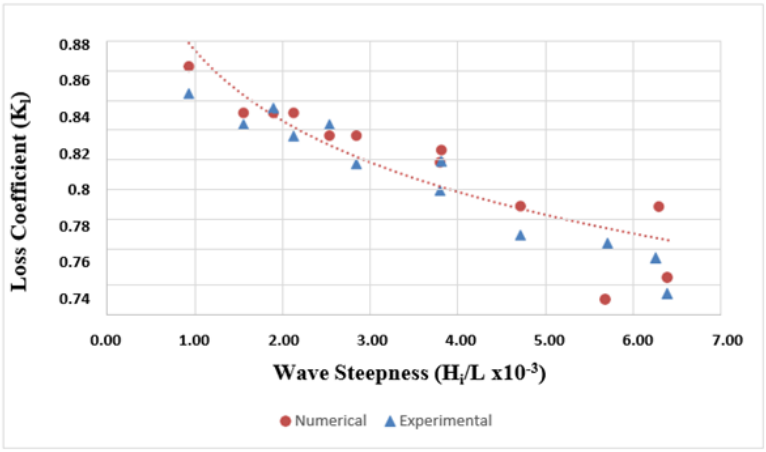

Fig. 18 Comparison of numerical and experimental loss coefficient (K_l) with Wave steepness (H_i/L), for d/hs =0.732

Similar to the numerical loss coefficient, the experimental loss coefficient also decreases with an increase in incident wave height for a given relative water depth and hence the dissipation is lesser for high wave steepness values. The experimental results are also found to be in good agreement with numerical results. The percentage error of numerical results from the experimental results varies between 2.3% to 7.1%, which is within the acceptable limit.

Similar to the numerical loss coefficient, the experimental loss coefficient also decreases with an increase in incident wave height for a given relative water depth and hence the dissipation is lesser for high wave steepness values. The experimental results are also found to be in good agreement with numerical results. The percentage error of numerical results from the experimental results varies between 2.3% to 7.1%, which is within the acceptable limit.

5.5.8 Flow field near the test model based on CFD

A typical result of the numerical flow field near the QCB (test model) for $H_i/d = 0.40$, T= 2.2 s is illustrated in Fig. 19 for t = 10 s, 20 s, 30 s. This flow nature helps in understanding the physics of the kinematics of water particle motion during the wave structure interaction. At the initial stage (i.e.,) the generation of the wave from the wave generating zone and the ensuing propagation of the wave toward the model before the wave starts interacting with the test model (Fig. 19(a)). Fig. 19(b) shows the fully developed wave interacting with the test model and the water particle velocities are

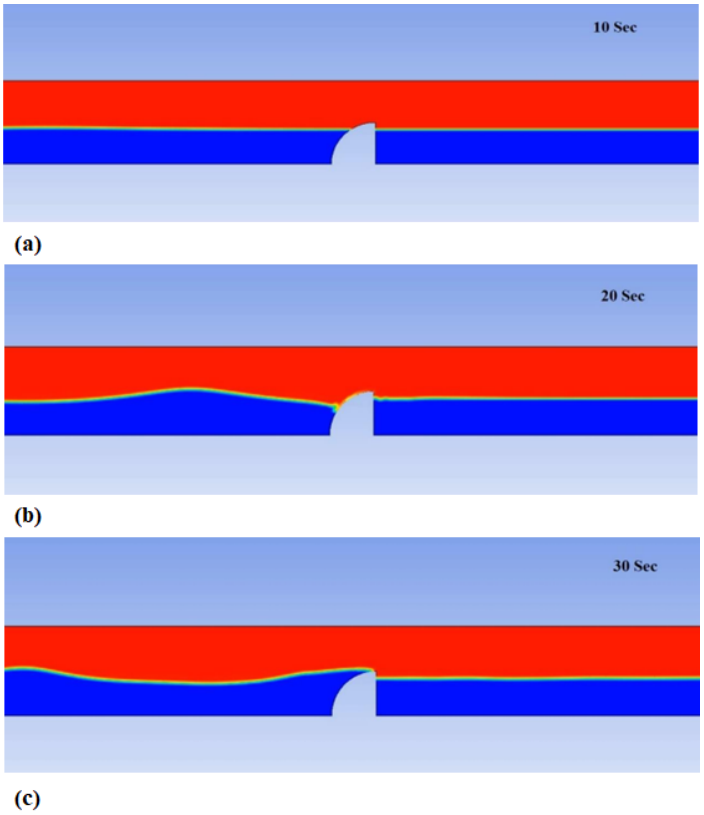

Fig. 19 Numerical flow field near test model with H_i/d =0.40, T=2.2 s

maximum at a fully developed wave crust location. On the other hand, the water depth is less than half of the wavelength, which implies the water particles move in an elliptical motion.

The backflow of water particles from the test model is observed when the structure attained maximum run-up (Fig. 19(c)). Similarly, the velocity of water particles is more at 20 sec when compared to the velocity of water particles at 10 s, which increases the run-up on the test model and subsequently the flow overtops on the tip of the test mode. As the time progresses, (i.e., for 25 sec – 30 sec) the wave impinges more on the breakwater and hence results in overtopping towards the lee side of the test model. From the outcome, it is evident that numerical results are having a good correlation with experimental findings as discussed in the earlier sections.

6. Conclusions

An attempt has been made to analyse the performances of the NWF by varying the beach slopes, length of NWF, and mesh sizes to arrive at optimum geometrical conditions for better numerical solutions. Finally, the recommended NWF is validated with the physical model study on the hydraulic performance of quarter circle breakwater (QCB).
Based on that the following conclusions have arrived:

1. Increasing the computational grid or mesh size results in wave damping and a small shift in the peak of results providing insignificant numerical solutions. To overcome these three mesh sizes (0.01 x 0.01. 0.02 m x 0.02 m and 0.03 m x 0.03 m) are considered. It is noted that (0.02 m x0.02 m) agrees with experimental and theoretical approaches and is effective in computational time compared to a lower mesh size (0.01 m x 0.01 m). NWF doesn't significantly affect varying beach slopes concerning the mesh size.
2. The beach slopes of (1:3, 1:5, and numerical beach conditions) are implemented in the downstream end of NWF to address the wave reflection and concluded that the beach slope of 1:5 and numerical beach conditions are similar in the performance of wave absorbing nature. In addition, a 36 % reduction in the simulation time is observed in the case of numerical beach conditions.
3. To optimize the length of NWF, several factors are considered. Finally, the numerical simulations with a mesh size of 0.02 m x 0.02 m, with timestep 0.01 s, 20 m NWF length, and numerical beach condition provide a good output with an excellent agreement with theoretical and experimental results.
4. Eventually, it is noted that the prediction by CFD results is compared very well with the measured wave reflection coefficient (Kr), wave runup (R_u/H_i) and with energy loss coefficients (K_l) for a range of input conditions consider in the study. The CFD results compare satisfactorily with the experimental results.

Acknowledgments

The authors are thankful to the Dr. R.S. Kankara, Director, CWPRS for providing direction to this work. The authors express gratitude to Central Research Facility, NITK, for providing access to ANSYS software.

Conflict of Interest

The authors declare that they have no known competing financial interests or personal relationships that could have appeared to influence the work reported in this paper. The authors declare that they have no conflict of interest.

CRediT author statement

Kumaran: Conceptualization, Original Draft Preparation, Methodology, CFD simulations and Investigation. **A.V Mahalingaiah:** Investigation and Supervision**. Manu** Data Curation, Formal Analysis and Investigation. **Subba Rao:** Supervision.

Funding

There is no funding source.

References

ANSYS-Inc. (2020), ANSYS FLUENT, Release 20.1.

Binumol, S., Rao, D. and Hegde, A.V. (2017), "Hydrodynamic performance characteristics of an emerged perforated quarter circle breakwater", *Int. J. Innov. Res. Sci. Eng. Technol*., **6**(4), 45-48.

Chakrabarti, S.K. (1994), Offshore Structure Modelling, World Scientific, Singapore.

Chang, J.Y., Lin, Y.T. and Tsai, C.C. (2018), "Viscous numerical wave tank for Bragg resonance by cnoidal and Stokes waves", *Eng. Appl. Comput. Fluid Mech*., **12**(1), 308-323. https://doi.org/10.1080/19942060.2018.1432507.

Cointe, R. and Geyer, P. (1991), Nonlinear and linear motions of a rectangular barge in a perfect fluid.

Dean, R.G. and Dalrymple, R.A. (1984), Water Wave Mechanics for Engineers and Scientists, Prentice-Hall, Englewood Cliffs, New Jersey.

Elangovan, M. (2011), "Simulation of irregular waves by CFD", *Int. J. Mech. Aerosp. Ind. Mechatr. Manuf. Eng*., **5**(7), 1379-1383.

Finnegan, W. and Goggins, J. (2012), "Numerical simulation of linear water waves and wave structure interaction", *Ocean Eng*., **43**, 23-31. https://doi.org/10.1016/j.oceaneng.2012.01.002.

Galvin, C.J.J. (1964), Wave-height prediction for wave generators in shallow water. Tech. Memo. 4 (US Army Coastal Engineering Research Center).

Goda, Y. and Suzuki, Y. (1976), "Estimation of incident and reflected waves in random wave experiments", *Proceedings of the 15th Coastal Engineering Conference*, Honolulu, Hawaii.

Hajivalie, F., Yeganeh Bakhtiary, A. and Javan, A.H. (2007), "Numerical study of vertical breakwater influence on the breaking wave", *Proceedings of the International Conference on Violent Flows*, Organized by RIAM, Kyushu University, Fukuoka, Japan.

Havn, J. (2011), "Wave loads on underwater protection covers", Master's thesis, Dept of Marine Technology, NTNU.

Hu, Z.Z., Greaves, D. and Raby, A. (2016), "Numerical wave tank study of extreme waves and wave-structure interaction using Open Foam", *Ocean Eng*., **126**, 329-342. https://doi.org/10.1016/j.oceaneng.2016.09.017.

Issacson, M. (1991), "Measurement of regular wave reflection", *J. Waterw. Port C. - ASCE*, **117**(6), 553-569. https://doi.org/10.1061/(ASCE)0733-950X(1991)117:6(553).

Kandula, J., Usha Sri, P., Ravinder Reddy, P. and Gugulothu, S.K. (2022), "Numerical and experimental

evaluation of near-wake cavitation flow around axisymmetric cavitators", *Ships Offshore Struct*., **17**(5), 1042-1052. https://doi.org/10.1080/17445302.2021.1893458.
Kariem, A.S.I. (2016), "Proposing and investigating the efficiency of vertical perforated breakwater", *Int. J. Sci. Eng. Res*., **7**(3),
Krishna, P., Roopsekhar, M., Sundar, V., Sundaravadivelu, R. and Graw, K.U. (2000), "Hydrodynamic pressures on submerged semicircular breakwaters", *Proceedings of the International Conference on Coasts, Ports and Marine structures*, Iran, Bandar Abbas,21-24, November.
Kumaran, V., Neelamani, S., Vijay, K.G., Al-Anjari, N. and Al-Ragum, A. (2022), "Wave attenuation by multiple slotted barriers with a zig-zag arrangement -A physical and numerical approach", *J. Hydro-Environ. Res*., **41**, 25-37. https://doi.org/10.1016/j.jher.2022.02.001.
Lal, A. and Elangovan, M. (2008), "CFD simulation and validation of flap type wave-maker", *Int. J. Math. Comput. Phys. Electr. Comp. Eng*., **2**(10), 708-714.
Le Mehaute, B., Divoky, D. and Lin, A. (1968), "Shallow water waves a comparison of theories and experiments", *Coast. Eng*., 86-107. https://doi.org/10.1061/9780872620131.007.
Liang, X.F., Yang, J.M., Li, J., Xiao, L.F. and Li, X. (2010), "Numerical simulation of irregular wave-simulating irregular wave train", *J. Hydrodyn. Ser. B*., **22**(4), 537-545. https://doi.org/10.1016/S1001-6058(09)60086-X.
Machado, F.M.M., Lopes, A.M.G. and Ferreira, A.D. (2018), "Numerical simulation of regular waves: Optimization of a numerical wave tank", *Ocean Eng*., **170**, 89-99. https://doi.org/10.1016/j.oceaneng.2018.10.002.
Maguire, A.E. (2011), Hydrodynamics, Control and Numerical Modelling of Absorbi Wavemakers. The University of Edinburgh.
Mansard, E.P.D. and Funke, E.R. (1987), On the reflection analysis of irregular waves. Technical Report TR-HY-017, NRCC, No. 27522. National Research Council of Canada, Canada.
Manu, V.K. and Rao, S. and Reddy, I.S. (2021), "Hydrodynamic performances of a wall type breakwater - a physical and numerical approach", *J. Naval Architect. Marine Eng*., **18**(2), 141-154.
Nizamani, M., Nizamani, Z., Nakayama, A. and Osman, M. (2021), "Analysis of loads caused by waves on the deck near the free surface of the offshore platform using CFD", *Ships Offshore Struct*., **17**(9), 1964-1974. https://doi.org/10.1080/17445302.2021.1954329.
Silva, M.C., Vitola, M. de A., Pinto, W.T. and Levi, C.A. (2010), "Numerical simulation of monochromatic wave generated in laboratory: Validation of a CFD code", *Proceedings of the Atas do 23º Congresso Nacional de Transporte Brasil*.
Wang, W., Kamath, A., Martin, T., Pákozdi, C. and Bihs, H. (2020), "A comparison of different wave modelling techniques in an open-source hydrodynamic framework", *J. Mar. Sci. Eng*., **8**(7), 526. https://doi.org/10.3390/jmse8070526.
Yuan, D. and Tao, J. (2003), "Wave forces on submerged, alternately, submerged, and emerged semicircular breakwaters", *Coast. Eng. J*., **48**(2), 75-93. https://doi.org/10.1016/S0378-3839(02)00169-2.
Zelt, J.A. and Skjelbreia, J.E. (1992), "Estimating incident and reflected wave fields using arbitrary number of wave gauges", *ASCE, Coastal Eng*., 777-789. https://doi.org/10.1061/9780872629332.058.
Zhang, H.C., Liu, S., Li, J. and Wang, L. (2019), "Establishment of numerical wave flume based on the second-order wave-maker theory", *China Ocean Eng*., **33**, 160-171. https://doi.org/10.1007/s13344-019-0016-6.
Zhu, S. (1999), "Separation of regular waves by a transfer function method", *Ocean Eng*., **26**(12), 1435-1446. doi:10.1016/S0029-8018(98)00041-9.

Nomenclature

d	Water depth
S	Stokes length
CFD	Computational Fluid Dynamics
QCB	Quarter Circular Breakwater
NWF	Numerical Wave Flume
ω	Angular Frequency
k	Wavenumber
L	Wavelength
H	Wave height
T	Wave period
FFT	Fast Fourier Transform
BEM	Boundary Element Method
SBW	Semi-Circular Breakwater
N-S	Navier-Stokes
g	Acceleration due to gravity
s	Scaling factor
μ	Viscosity
K_r	Wave reflection
UDF	User-Defined Function
VoF	Volume of Fluid